ADVANCED MATERIALS INTERFACES

www.advmatinterfaces.de

Photoinduced Orientation-Dependent Interlayer Carrier Transportation in Cross-Stacked Black Phosphorus van der Waals Junctions

Wei Xin, Hao-Bo Jiang, Xiao-Kuan Li, Xiang-Feng Zhou, Jin-Long Lu, Jian-Jun Yang, ChunLei Guo, Zhi-Bo Liu,* and Jian-Guo Tian*

A combination of different 2D layered materials by van der Waals (vdW) stacking or lateral splicing provides the basic building blocks for dynamic behavior researches of interlayer carriers. Anisotropic materials, recently, have further attracted attentions in this field because of their supply of freedoms for regulating the performance of electro-optical devices, whereas detailed characteristics and mechanisms of interlayer carrier transportation in these materials need remain to be revealed. Here, by using the photoassisted field effect and scanning photocurrent imaging measurements, it is demonstrated that the photoinduced interlayer carrier transportation in cross-stacked black phosphorus (BP) vdW junctions is strongly dependent on the crystal orientation and stacking morphology. Type-I and II band alignments are respectively predicted in the BP junctions with parallel and vertical crystal orientation stacking. The interlayer carrier transportation with both vertical and lateral modes is observed within only one sample. Combined first principle calculation with band theory analyses, the small band offset for holes and tunneling effect play key roles during the interlayer transportation. These results highlight the importance of crystal orientation of materials in vdW junctions and provide insights, both experimentally and theoretically, into engineering and design of orientation-based nanodevices.

2D layered materials, such as graphene, hexagonal boron nitride, and transition-metal dichalcogenides (TMDs), have attracted great attentions due to the amazing electrical and optical properties modification in low-dimensional space.[1,2] Recently, these tuning possibilities were increased thanks to vertical stacking of different 2D materials, layer-by-layer, to form van der Waals heterostructures (vdWHs), or splicing in-plane to form lateral ones. The new paradigms emerge with respect to both architectures to research, engineer, and manipulate the properties of interlayer carriers.[3,4] However, the influence of crystal structure of materials in these architectures has rarely been investigated intensely, which will be magnified especially in low-dimensional anisotropic materials, black phosphorus (BP) for instance.[5,6] As a new 2D layered material with puckered structures, BP recently unveiled highly desirable properties for application such as high carrier mobility, thickness-dependent tunable direct band gap, broad spectrum absorption, and the unique in-plane anisotropic properties.[7,8] Large anisotropy, which can be observed through effective mass, band structure etc., was found along different crystal orientations.[9–12] This offers another degree of freedom for the design of novel vdW nanodevices.[13] Therefore, an in-depth understanding of the influence of both crystal structure and vdW stacking morphology on the photoelectric properties is highly desirable for further development.

In this paper, we present the photoelectric properties of BP, with or without another piece on it, using both the photoassisted field-effect and scanning photocurrent imaging (SPI) methods.[14] The SPI measurement provides detailed information about the spatial distribution of the built-in electric field and the generation and recombination of photoinduced carriers, which is helpful for the analysis of interaction of interlayer carriers.[15] In our experiments, the orientation of top BP (TBP) in vdW structures has been changed from vertical to parallel to the bottom BP (BBP). Although the photoresponse, as indicated in the current–voltage (I–V) curves, is almost the same among the three samples, the response region shown in photocurrent image varies considerably, which strictly depends on the crystal orientation and the

Dr. W. Xin, Dr. X.-K. Li, Prof. X.-F. Zhou, Prof. Z.-B. Liu, Prof. J.-G. Tian
The Key Laboratory of Weak Light Nonlinear Photonics Ministry of Education
Teda Applied Physics Institute and School of Physics
Nankai University
Tianjin 300071, China
E-mail: liuzb@nankai.edu.cn

Dr. W. Xin, J.-L. Lu, Prof. J.-J. Yang, Prof. C. L. Guo
The Guo China-U.S. Photonics Lab
Changchun Institute of Optics
Fine mechanics, and Physics
Chinese Academy of Sciences
Changchun 130033, China
E-mail: guo@optics.rochester.edu

Dr. H.-B. Jiang
The Key Laboratory of Bionic Engineering Ministry of Education
Jilin University
Changchun 130023, China

Prof. C. L. Guo
The Institute of Optics
University of Rochester
NY 14627, USA

DOI: 10.1002/admi.201800964

stacking morphology. Especially in the BP vdW junctions with vertical orientation stacking (V-BPJ), both vertical and lateral interlayer carrier transportation are observed within only one sample for the first time. Using first principle calculation and band theory analysis, we attribute the interesting phenomena to the small band offset and tunneling effect.[16,17] These results will not only help clarify details about interlayer photoinduced carrier transport but also be expanded into other anisotropic low-dimensional materials, such as ReS_2 and GeP.[18,19]

A proof-of-concept V-BPJ sample was prepared on Si/SiO_2 substrate (see **Figure 1**a), using two pieces of exfoliated few-layered BP (≈5.2 and 4.8 nm) to produce a vertical architecture. Metal electrodes (5/50 nm Ti/Au) were then deposited using photoetching and magnetron sputtering, and marked as T1, T2, B1, and B2, respectively. The corresponding optical microscopy (OM) and schematic of the cross section of V-BPJ from different perspectives are also presented. We only connected the opposite electrodes of one of the BP samples as source and drain in the circuit, and the other sample just played a contact role. Although only one sample is connected to the circuit, another contact one is enough to have a critical effect on the optoelectronic performance of the vdW junction.[20] Carriers transport between electrodes needs to be affected by different crystal structures and thicknesses of BP, which is the main difference from conventional BP electrical devices. The interaction between TBP and BBP will affect the entire system under such conditions. The detailed preparation process and corresponding characterizations of V-BPJ are shown in Figures S1–S4 in the Supporting Information.

For deep insights into the electrical and optical characteristics of V-BPJ, measurements were carried out with and without laser irradiation. Figure 1b,c respectively shows the source–drain *I–V* curves and the p-type switching behaviors (inset) with the connection of T1 and T2, B1 and B2. Near linearization at low voltage (<1 V) and relatively high mobility in both connections (smaller than 578 and 450 $cm^2\ V^{-1}\ s^{-1}$, Figure S5, Supporting Information) have been observed.[21] When the sample was exposed to the laser illumination (532 nm, 1 mW), the typical dark and photocurrent measurements as a function of the source–drain bias in different circuit connection can be obtained, suggesting the photovoltaic effect plays a key role during this process, as shown in Figure 1e,f, where an inset presents normalized temporal photoresponse features.[22,23] The response time is only on the order of hundred milliseconds, and the rise time is generally shorter than the fall time. Then, if we change the polarization state and the power of the incident light, the photocurrent intensity can also be tuned gradually.[24] Due to the unique band structure and optical selection rules, the armchair (AC)-polarized incident light (the polarization is parallel to the BP's AC crystal orientation) can be absorbed totally, whereas the zigzag (ZZ)-polarized light can only be absorbed partially.[25] This results in the optical linear dichroism of BP and in turn leads to strong in-plane anisotropic photocurrent characteristics. The photocurrent anisotropy ratio (σ) and photoresponsivity along T1–T2 direction are respectively 0.24 and 2.1 mA W^{-1}, while along the B1–B2 direction are 0.41 and 0.8 mA W^{-1} (Figure S6, Supporting Information). Interestingly, since the orientation of TBP is perpendicular to BBP in V-BPJ

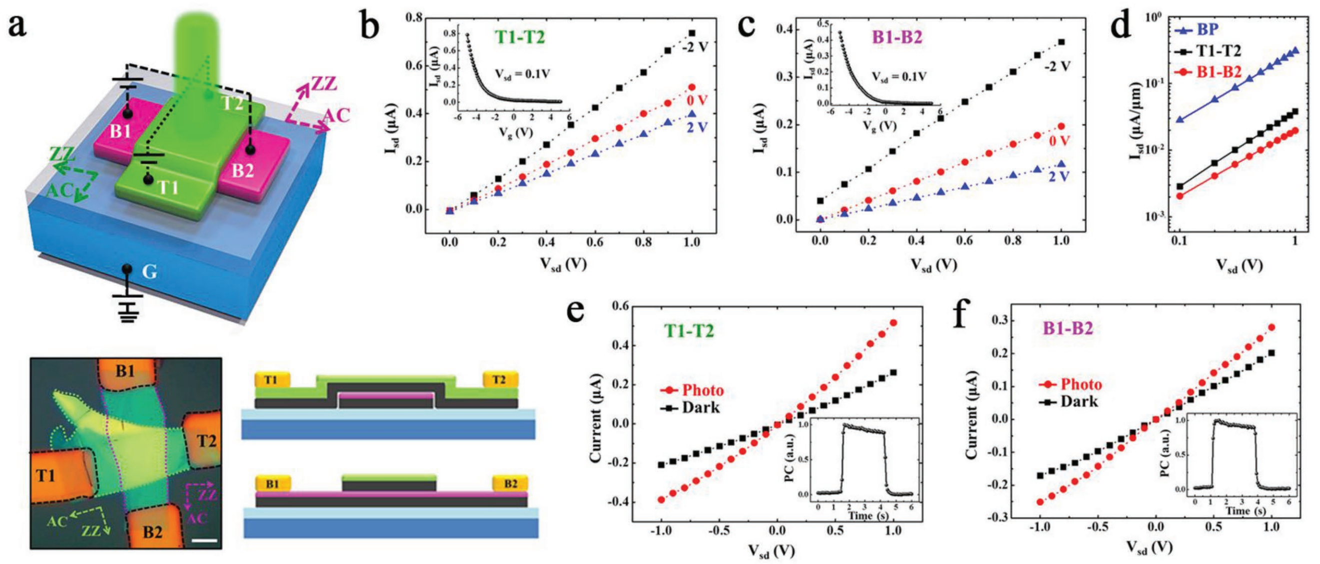

Figure 1. Schematic illustration, optical image, and photoelectric properties of V-BPJ. a) Up: Schematic illustration of V-BPJ. The few-layer BPs (FL-BPs) are respectively depicted in green (TBP) and pink (BBP). The crystal orientations along armchair (AC) and zigzag (ZZ) directions are marked. The opposite electrodes are defined as source and drain, and the silicon substrate is defined as back-gate. Down left: Optical image of V-BPJ. The TBP and BBP are outlined in green and pink just corresponding to the schematic. The gold electrodes are marked as T1, T2, B1, B2, respectively. Scale bar is 5 µm. Down right: Side views of V-BPJ along the directions of T1–T2 and B1–B2. The top-down materials are gold electrodes, TBP, BBP, SiO_2 and Si, respectively. The TBP (BBP) is composed of green (pink) phosphorus oxide film and BP (Figure S1, Supporting Information). b,c) The gate tunable linear *I–V* characteristics (main) and transfer curves (inset) of V-BPJ under different connections. d) Electrical properties comparison between V-BPJ and conventional BP junction (Figure 3a). e,f) Main: *I–V* characteristics of V-BPJ with and without laser illumination (532 nm, 1 mW) under different connections. Inset: Normalized temporal photoresponse intensity features. All the photoresponse shown here are the maximum values obtained after adjusting the polarization states of incident light.

samples, the absorption of the same incident light will be different between TBP and BBP. Hence, different from traditional phenomena occurring on BP-only field-effect transistors (FET, named as BP junction), the polarization-dependent photoresponse of V-BPJ here is a "whole" effect for consideration both the response of TBP and BBP. The incident polarization states will affect V-BPJ's interlayer carrier transportation. The strong interlayer coupling in overlapping domain has attenuated the current by one order of magnitude, as shown in Figure 1d.

Moreover, in order to further explore the photoinduced orientation-dependent interlayer carrier transportation in V-BPJ geometry, SPI was performed to obtain the spatial distribution of photoinduced carriers generation and recombination.[14,15] The scanning area focused on the same position including the overlap between TBP and BBP as well as the connection area between BP and electrodes, as shown in Figure 1a. Only T1 and T2 electrodes and B1 and B2 are connected as source and drain in the circuit, which are corresponding to the scanning results shown in **Figure 2**a,b. The polarization states of incident light have been marked as white arrows.

By comparing the experimental data, some points have caught our attentions. First, the photocurrent intensities are unevenly distributed within the same scanning area. The strongest position is mostly concentrated around the interface, no matter between TBP and BBP, or BP and electrodes. This phenomenon has been reported in previous works. The photocurrent distribution is mainly affected by the surface charge transfer doping effect, which relies on the interfacial interaction caused by the energy band bending.[5] However, without extra voltage application, the most interesting results are the discrepant SPI images when the same samples are just connected between different electrodes. The strongest photoresponse occurs covering the TBP/BBP overlapping domain when connecting T1 and T2, whereas the strongest signals were observed at the TBP/BBP interface for B1–B2 connection (red dotted frames in Figure 2a,b). The latter phenomenon has been seen in most vertical vdWHs but the former is almost never reported.[26,27]

To illustrate the effect of gate and bias voltage on V-BPJ, the first principles calculation and energy band theory are

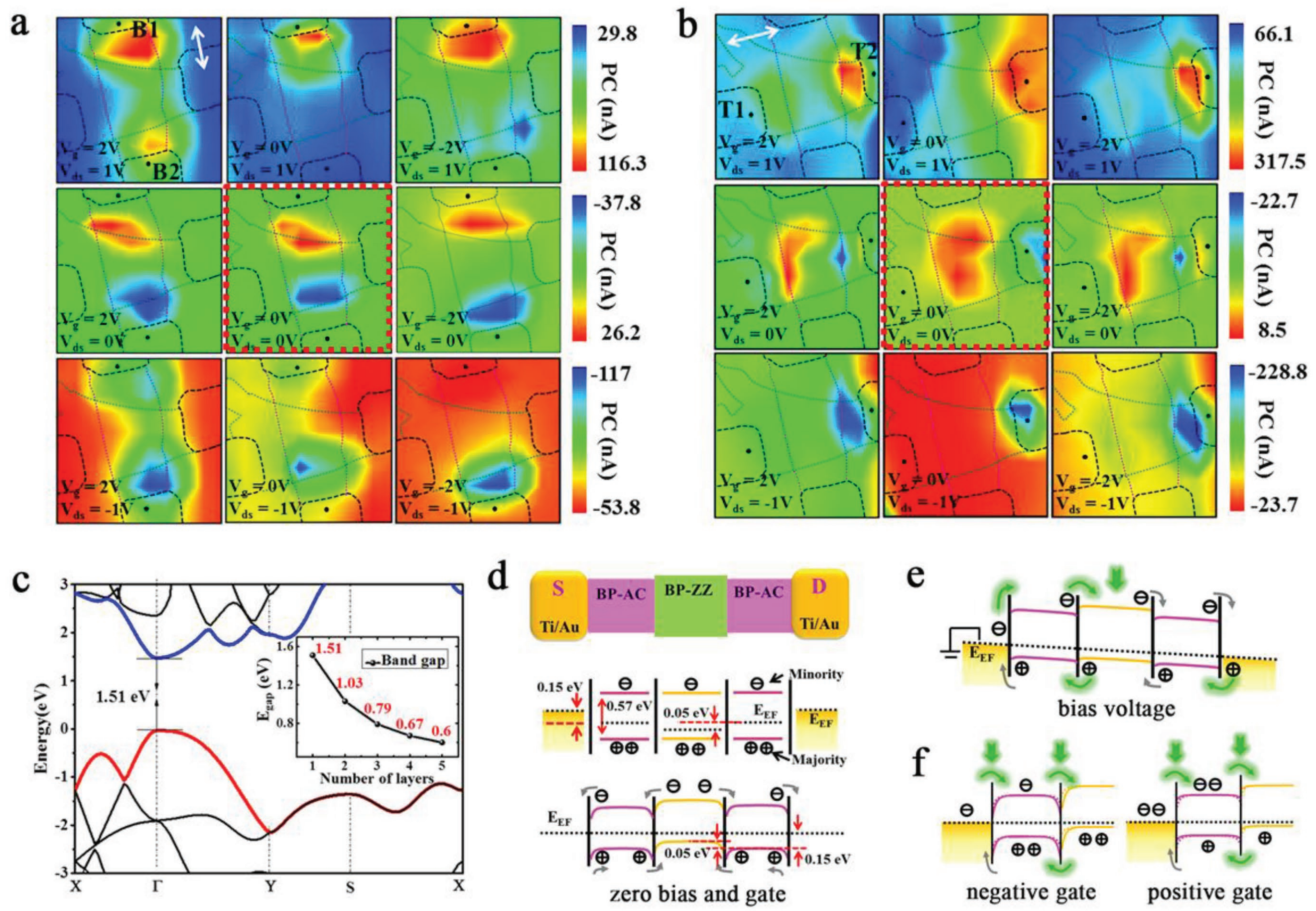

Figure 2. SPI measurements and band analysis of V-BPJ. a,b) SPI measurements of V-BPJ with different gate and source–drain bias voltages under B1–B2 and T1–T2 connections, respectively. The scanning area is almost identical to the position of the image in Figure 1a. The wavelength and power of incident laser is 532 nm and 1 mW. The polarizations are also marked as white arrows. The focused SPI images without voltages treatment are outlined with red dotted lines. c) Main: Band structure of single-layer BP calculated by HSE06 function. The blue and red lines represent the conduction and valence band, respectively. Inset: The variable band gap as a function of the thickness of few-layer BP. d–f) Schematic and band diagrams of V-BPJ under different conditions. Type II band alignment is shown at the TBP/BBP interface.

considered. With the HSE06 functional (optB88-vdW), a direct band gap of 1.51 eV at Γ point of single-layered BP and significant asymmetric band dispersion along Γ–X and Γ–Y branches could be observed.[10,11] When the BP layer number increases from one to five, the gap decreases rapidly to about 0.57 eV, as shown in Figure 2c (Figures S7 and S8, Supporting Information). However, when the layer increases further, the variation trend of band gap becomes weak. Both calculations and transport measurements have already confirmed this feature.[28] Therefore, even if the thicknesses of the BP samples are slightly different in our experiments, it does not hinder the theoretical predictions. To simplify the analysis, the BP samples used here are all considered to consist of five layers.

Figure 2d illustrates the schematic and band diagrams of V-BPJ under zero bias and gate application, respectively. At the BP/metal interface, a work function of BP that is about 0.15 eV higher than the Ti/Au electrode produces lower electronic energy and forms a Schottky barrier after connecting.[11] The band bending can occur here and generates a built-in electric field pointing from BP to electrodes. Similar bending at the overlapping region in V-BPJ can also be seen. Somewhat differently, the variation of thickness and crystal orientation should be taken into account at this point. Based on previous reports, the orientation barrier (OB) that is caused by the anisotropic band distribution along different orientations in BP, plays a more important role.[13] The type II band alignment forms and results in a built-in potential pointing from AC to ZZ directions. The band offset caused by OB is about 0.05 eV. Despite all this, the back-to-back junction structures result in a symmetric band distribution, which still limits the unidirectional transport of carriers when there is no extrinsic stimulus.[29,30] This balance cannot be broken until the sample is exposed under the laser stimulation. The photoinduced carriers generate and can be driven by the built-in electric field to enhance the photoresponse. Due to the small barriers no matter at the interface of BP/metal or TBP/BBP, tunneling effect can play a key role. Therefore, under the interaction of OB and tunneling, no matter majority carriers (holes) transport along B1–B2 or T1–T2 directions, similar transport process (AC-ZZ-AC) needs to be experienced. When the V-BPJ is irradiated under the connection between T1 and T2 electrodes, the generation and recombination of photoinduced carriers mainly distributes in the overlapping domain, mainly resulting in the vertical interlayer carrier coupling.[14,31] But in the cases of B1–B2 connection in V-BPJ, the photocurrent enhancement mainly occurs near the interface between TBP and BBP, which more likes a lateral coupling.[32,33] Due to the different stacking morphology along different directions, the carrier transportation paths change, which further leads to a discrepant photocurrent distributions.

In addition to the aforementioned property, the voltage tunable phenomenon should also be emphasized. When we tuned the gate (V_g) and source–drain voltages (V_{ds}), the SPI results could also be changed slightly. In general, as for gate voltage, it can directly modulate the carrier density and the Fermi level distribution of samples, which can result in a total higher or lower barrier formation.[34] Unlike gate tuning, the variation of bias voltage can provide a directional electric field to the sample and push the carriers to move directionally (Figure 2e,f). Meanwhile, it also changes the contact potential difference at the interface causes a considerable change of the built-in electric field. That means when you increase the bias voltage gradually, the energy band will move up (forward) or down (reverse).[13]

Here, we found that the effect of the gate and bias voltage has a great influence on the photocurrent distribution of V-BPJ, even if the applied voltage is small (–1 to 1 V for V_{ds}, –2 to 2 V for V_g). This is mainly because the height of the Schottky barrier at the BP/metal interface is much larger than OB. Under the action of the voltage, the influence of OB has been weakened. As a result, the bias voltage makes the photocurrent distribution move toward the electrodes and the gate voltage causes a little rectification (Figures S9 and S10, Supporting Information). This also illustrates from another side that the effect of crystal orientation is an "intrinsic" factor affecting the interlayer carrier transportation in the vdW structures. In addition, apart from the photovoltaic, tunneling, influence of barriers and applied voltage mentioned above, the photogating effect may also need to be considered.[35] It can modulate the source-drain channel conductance and further influence the interlayer carriers transportation of VBP by inducing an additional 'electric field' just like another gate voltage. The comprehensive interaction of multiple effects leads to the complex interlayer carrier transportation.

In order to verify the above hypothesis, similar SPI measurements were conducted on another two types of BP samples. One sample is the BP device which is based on a traditional back gate FET configuration (BP junction).[21] It is beneficial for us to clarify the impact of stacking morphology on the generation and recombination distribution of the photoinduced carriers. Another sample is also the BP vdW junctions but with parallel crystal orientations between TBP and BBP (P-BPJ). This discrimination helps to reveal whether the interlayer carrier transportation is affected by a change in the orientation of 2D anisotropic materials. The preparation procedure, circuit connection, and laser illumination conditions are similar for all the above samples.

Figure 3a,b shows the schematic diagram, OM image, and SPI results of BP junction, respectively. Unlike the SPI measurements in V-BPJ, only two photocurrent peaks with opposite signs can be observed at the interface between BP and electrodes at different gate voltages. We attribute this to the affection of local electric fields caused by Schottky barrier.[5] The detailed band analysis is shown in Figure 2d. Because of the back-to-back structure, photoinduced carriers can be driven by the built-in electric field to enhance the photoresponse but cannot change the current transmission. This is why the photoresponse enhancement with opposite signs can only be observed at the interface in SPI images, but the rectified *I–V* curves cannot be obtained. The effect of the barrier here is clearly highlighted in BP junctions but overwhelmed in V-BPJ. That means that the energy band alignment is significantly affected by stacking morphology.

This conclusion can be further verified with the SPI measurements in P-BPJ, as shown in Figure 3d. The corresponding OM images and schematic are presented in Figure 3c. The strongest positions with regard to photoresponse for different gate voltages are all focused near the interface between TBP and BBP rather than the metal-BP edges. However, the photoresponse

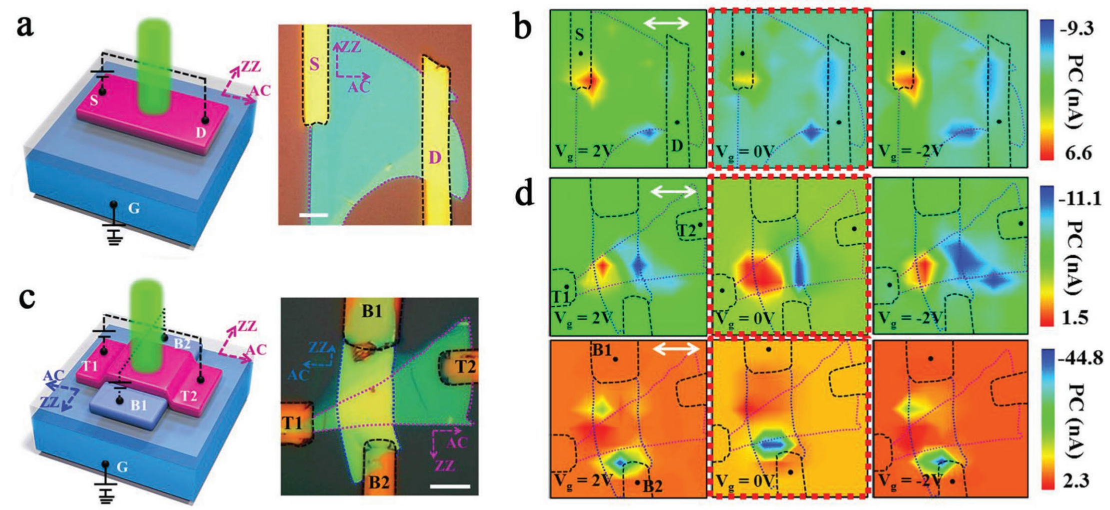

Figure 3. Schematic, OM images, and SPI measurements of BP junction and P-BPJ. a,c) Schematic and photos of BP junction and P-BPJ with 532 nm laser irradiation under different circuit connections. The electrodes and crystal orientations of BP are marked. The FL-BP is also presented as pink. In order to distinguish the difference between V-BPJ and P-BPJ, the other FL-BP is presented as blue (BBP in P-BPJ). The samples in OM images are also outlined in corresponding colors. All the scale bars are 10 µm. b,d) SPI measurements of BP junction and P-BPJ at different gate voltages. The incident polarization states are also marked.

enhancement at TBP/BBP junction domain cannot be observed any more regardless of carrier transport conditions. This indicates that crystal orientation is a non-negligible factor, which can greatly affect the transportation of the interlayer photoinduced carriers in anisotropic material-based vdW structures. Detailed preparation process and photoresponse information about the BP junction and P-BPJ is shown in Figures S1 and S11 in the Supporting Information. Furthermore, the band distribution is considered. Figure S8c in the Supporting Information shows the structure and band diagram of the overlapping domain, respectively. Because the crystal orientation between TBP and BBP are almost the same, the differences in thickness are the only factor for consideration regardless whether the carriers transport in the direction of B1–B2 or T1–T2.[36] After the band theory analysis based on previous studies, a band offset about 0.14 eV for holes forms at the TBP-BBP interface (Figure S8, Supporting Information).[10,11,37] This results in a type I band alignment and both electrons and holes are injected into the overlapping domain. Similar conclusion has also be drawn in previous study (all-BP lateral heterojunction diode).[29] The current driven by the external electric field flows mostly via the BBP.[38] However, if the P-BPJ is exposed to laser illumination, the balance is no longer maintained due to the dramatic increase of photoinduced carriers. The smaller band offset at the overlapping domain makes it possible to permit holes to tunnel from multilayer to few-layered BP.

As a result, from above analyses we can draw the following conclusion: the BP' crystal orientation and stacking morphology in its vdW structures have a great influence on the interlayer carrier transportation. For P-BPJ, the built-in electric field caused by the thickness-dependent barrier plays a major role in carrier migration. For V-BPJ, the interlayer carriers transportation will be more affected by the "OB," which may result in the selective transport routes of carriers. **Figure 4**a,b shows the ideal interlayer carrier transportation modes in P-BPJ and V-BPJ on cross-sectional and 3D view, respectively. The carriers will pass through the entire sample of P-BPJ no matter what circuit connection, whereas experience a different process in V-BPJ. When the B1 and B2 electrodes are connected, at the overlapping region, carriers will mainly transport in the TBP. When T1 and T2 are connected, carriers will transport through the interface from TBP to BBP more easily. This discovery is a constructive

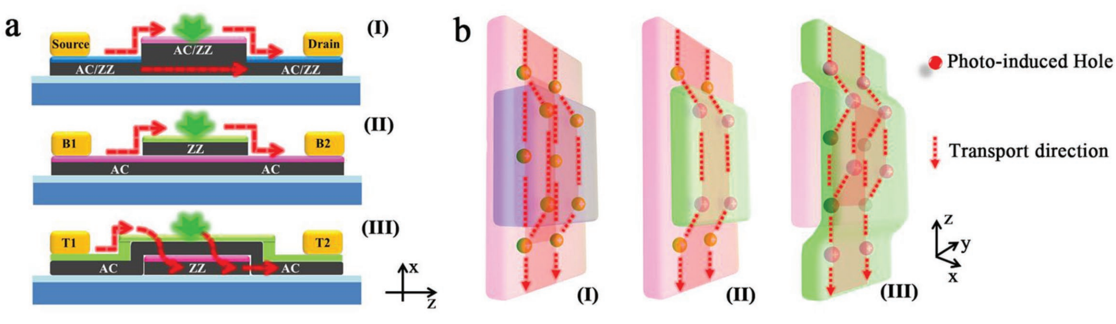

Figure 4. a,b) The ideal interlayer carrier transportation modes in P-BPJ and V-BPJ under cross-sectional and 3D view.

inspiration for us to regulate the properties of anisotropic material-based devices by changing the crystal orientations. Combine with the existing regulation techniques and the construction of special structures, new approaches for the development of 2D material-based photoelectric devices have been provided.[39,40]

In conclusion, by using SPI measurements, we have demonstrated that crystal orientation has a great effect on the interlayer transportation of photoinduced carriers in cross-stacked BP vdW junctions. Based on first principle calculation and band theory analysis, type I and II band alignments were predicted in P-BPJ and V-BPJ, respectively. A small band offset for holes and the interlayer tunneling effect provide theoretical support for the different carrier transport modes. Our work sheds light on the photoinduced interlayer charge transportation for the family of anisotropic materials-based vdW junctions. The results may open pathways for the design and preparation of novel optoelectronic nanodevices.

Experimental Section

Device Fabrication: The few-layered BP materials were all mechanically exfoliated using 3M tapes onto SiO_2/Si (285 nm) substrates from bulk materials (XFNANO, XF161). Traditional wetting transfer method was operated for making the vdW structures. Subsequently, metal electrodes (5/50 nm Ti/Au) were deposited by using the photoetching and magnetron sputtering technology. The thermal annealing treatment (340 °C for 1 h) in vacuum was also operated for close contact. The morphology, thickness and crystal orientation of samples were characterized by optical, atomic force microscope (Nanoscope Dimension 3100) and Raman spectrometer (RENISHAW RM2000, 514 nm), respectively.

Orientation Determination of BP Samples: The crystal orientation of BP sample is mainly determined by a homemade polarized optical microscope measurement system. The principle is based on the anisotropic optical absorption of BP. The experimental light path is similar to the Raman measurement. The only difference is that a charge coupled device (CCD) camera is used for recording the morphology of materials and an image software (ImageJ) is used for analyzing the polarization-dependent color contrast the samples. The detailed information can be seen in Figures S3 and S4 in the Supporting Information.

Photoelectric Properties Measurement: The photoelectric properties of different BP samples were measured by a homemade four-point-probe system.[13] The incident light source was provided by a continuous semiconductor laser (CNI, MGL-III-532, 532 nm). The polarization can be tuned gradually by a polarizer and $\lambda/4$ wave plate in the optical path. The laser was incident through a $\times 50$ objective lens, which can focus the beam size is less than 5 µm. The scanning position was precisely controlled and monitored by a galvanometer (SUNNY TECHNOLOGY, S-8316D) and a commercial digital camera CCD (OPTEC, TP310), respectively. The electrical signals were measured by digital sourcemeters (KEITHLEY 2400, 2450), which were also verified by another semiconductor characteristic analyzer (AGILENT, B1500A).

The First Principle Calculation: The first principle calculation was used the Vienna ab initio Simulation Package code. The generalized gradient approximation was used for density functional theory calculation. The optB88 exchange (optB88-vdW) and HSE06 hybrid functional were used for results optimization.

Supporting Information

Supporting Information is available from the Wiley Online Library or from the author.

Acknowledgements

This research was supported by the Natural Science Foundation of China (Grant No. 11774184), the Scientific Research Project of the Chinese Academy of Sciences (Grant No. QYZDB-SSW-SYS038), the National Key Research and Development Program of China (Grant No. 2016YFA0301102), and the National Postdoctoral Program for Innovative Talents, Natural Science Foundation of China (Grant No. BX201600064).

Conflict of Interest

The authors declare no conflict of interest.

Keywords

anisotropy, black phosphorus, interlayer carrier transportation, scanning photocurrent imaging measurement, van der Waals junction

Received: June 26, 2018
Revised: July 27, 2018
Published online: August 14, 2018

[1] F. Xia, H. Wang, D. Xiao, M. Dubey, A. Ramasubramaniam, *Nat. Photonics* **2015**, *8*, 899.
[2] C. Tan, X. Cao, X. Wu, Q. He, J. Yang, X. Zhang, J. Chen, W. Zhao, S. Han, G. Nam, M. Sindoro, H. Zhang, *Chem. Rev.* **2017**, *117*, 6225.
[3] A. Geim, I. Grigorieva, *Nature* **2013**, *499*, 419.
[4] Y. Gong, J. Lin, X. Wang, G. Shi, S. Lei, Z. Lin, X. Zou, G. Ye, R. Vajtai, B. Yakobson, H. Terrones, M. Terrones, B. Tay, J. Lou, S. Pantelides, Z. Liu, W. Zhou, P. Ajayan, *Nat. Mater.* **2014**, *13*, 1135.
[5] Z. Hu, Z. Wu, C. Han, J. He, Z. Ni, W. Chen, *Chem. Soc. Rev.* **2018**, *47*, 3100.
[6] X. Liu, Q. Guo, J. Qiu, *Adv. Mater.* **2017**, *29*, 827.
[7] F. Xia, H. Wang, Y. Jia, *Nat. Commun.* **2014**, *5*, 4458.
[8] A. Carvalho, M. Wang, X. Zhu, A. Rodin, H. Su, A. Castro Neto, *Nat. Rev. Mater.* **2016**, *1*, 16061.
[9] X. Wang, A. Jones, K. Seyler, V. Tran, Y. Jia, H. Zhao, H. Wang, L. Yang, X. Xu, F. Xia, *Nat. Nanotechnol.* **2015**, *10*, 517.
[10] J. Qiao, X. Kong, Z. Hu, F. Yang, W. Ji, *Nat. Commun.* **2014**, *5*, 4475.
[11] Y. Cai, G. Zhang, Y. Zhang, *Sci. Rep.* **2014**, *4*, 6677.
[12] J. He, D. He, Y. Wang, Q. Cui, M. Bellus, H. Chiu, H. Zhao, *ACS Nano* **2015**, *9*, 6436.
[13] W. Xin, X. Li, X. He, B. Su, X. Jiang, K. Huang, X. Zhou, Z. Liu, J. Tian, *Adv. Mater.* **2017**, *30*, 1704653.
[14] L. Britnell, R. Ribeiro, A. Eckmann, R. Jalil, B. Belle, A. Mishchenko, Y. Kim, R. Gorbachev, T. Georgiou, S. Morozov, A. Grigorenko, A. Geim, C. Casiraghi, A. Castro Neto, K. Novoselov, *Science* **2013**, *340*, 1311.
[15] F. Xia, T. Mueller, R. Golizadeh-Mojarad, M. Freitag, Y. Lin, J. Tsang, V. Perebeinos, P. Avouris, *Nano Lett.* **2009**, *9*, 1039.
[16] T. Cao, Z. Li, D. Qiu, S. Louie, *Nano Lett.* **2016**, *16*, 5542.
[17] X. Liu, D. Qu, H. Li, I. Moon, F. Ahmed, C. Kim, M. Lee, Y. Choi, J. Cho, J. Hone, W. Yoo, *ACS Nano* **2017**, *11*, 9143.
[18] S. Sim, D. Lee, A. Trifonov, T. Kim, S. Cha, J. Sung, S. Cho, W. Shim, M. Jo, H. Choi, *Nat. Commun.* **2018**, *9*, 351.
[19] L. Li, W. Wang, P. Gong, X. Zhu, B. Deng, X. Shi, G. Gao, H. Li, T. Zhai, *Adv. Mater.* **2018**, *30*, 1706771.
[20] L. Ye, P. Wang, W. Luo, F. Gong, L. Liao, T. Liu, L. Tong, J. Zang, J. Xu, W. Hu, *Nano Energy* **2017**, *37*, 53.

[21] L. Li, Y. Yu, G. Ye, Q. Ge, X. Ou, H. Wu, D. Feng, X. Chen, Y. Zhang, *Nat. Nanotechnol.* **2014**, *9*, 372.
[22] M. Buscema1, D. Groenendijk, G. Steele, H. van der Zant, A. Castellanos-Gomez, *Nat. Commun.* **2014**, *5*, 4651.
[23] W. Xin, X. Chen, Z. Liu, W. Jiang, X. Gao, X. Jiang, Y. Chen, J. Tian, *Adv. Opt. Mater.* **2016**, *4*, 1703.
[24] T. Hong, B. Chamlagain, W. Lin, H. Chuang, M. Pan, Z. Zhou, Y. Xu, *Nanoscale* **2014**, *6*, 8978.
[25] H. Yuan, X. Liu, F. Afshinmanesh, W. Li, G. Xu, J. Sun, B. Lian, A. Curto, G. Ye, Y. Hikita, Z. Shen, S. Zhang, X. Chen, M. Brongersma, H. Hwang, Y. Cui, *Nat. Nanotechnol.* **2015**, *10*, 707.
[26] Y. Deng, Z. Luo, N. Conrad, H. Liu, Y. Gong, S. Najmaei, P. Ajayan, J. Lou, X. Xu, P. Ye, *ACS Nano* **2014**, *8*, 8292.
[27] J. Lu, A. Carvalho, J. Wu, H. Liu, E. Tok, A. Castro Neto, B. Özyilmaz, C. Sow, *Adv. Mater.* **2016**, *28*, 4164.
[28] V. Tran, R. Soklaski, Y. Liang, L. Yang, *Phys. Rev. B* **2014**, *89*, 235319.
[29] L. Wang, L. Huang, W. Tan, X. Feng, L. Chen, K. Ang, *Adv. Electron. Mater.* **2018**, *4*, 1700442.
[30] H. Yang, J. Heo, S. Park, H. Song, D. Seo, K. Byun, P. Kim, I. Yoo, H. Chung, K. Kim, *Science* **2012**, *336*, 1140.
[31] C. Lee, G. Lee, A. van der Zande, W. Chen, Y. Li, M. Han, X. Cui, G. Arefe, C. Nuckolls, T. Heinz, J. Guo, J. Hone, P. Kim, *Nat. Nanotechnol.* **2014**, *9*, 676.
[32] M. Li, Y. Shi, C. Cheng, L. Lu, Y. Lin, H. Tang, M. Tsai, C. Chu, K. Wei, J. He, W. Chang, K. Suenaga, L. Li, *Science* **2015**, *349*, 524.
[33] P. Sahoo, S. Memaran, Y. Xin, L. Balicas, H. Gutiérrez, *Nature* **2018**, *553*, 63.
[34] D. Li, M. Chen, Q. Zong, Z. Zhang, *Nano Lett.* **2017**, *17*, 6353.
[35] H. Fang, W. Hu, *Adv. Sci.* **2017**, *4*, 1700323.
[36] Y. He, A. Sobhani, S. Lei, Z. Zhang, Y. Gong, Z. Jin, W. Zhou, Y. Yang, Y. Zhang, X. Wang, B. Yakobson, R. Vajtai, N. Halas, B. Li, E. Xie, P. Ajayan, *Adv. Mater.* **2016**, *28*, 5126.
[37] J. Yang, R. Xu, J. Pei, Y. Myint, F. Wang, Z. Wang, S. Zhang, Z. Yu, Y. Lu, *Light Sci. Appl.* **2015**, *4*, e312.
[38] M. Bellus, M. Li, S. Lane, F. Ceballos, Q. Cui, X. Zeng, H. Zhao, *Nanoscale Horiz.* **2017**, *2*, 31.
[39] D. Li, B. Wang, M. Chen, J. Zhou, Z. Zhang, *Small* **2017**, *13*, 1603726.
[40] D. Li, M. Chen, Z. Sun, P. Yu, Z. Liu, P. Ajayan, Z. Zhang, *Nat. Nanotechnol.* **2017**, *12*, 901.